Research Article | Vol. 30, No. 24 / 21 Nov 2022 / Optics Express 43491
Optics EXPRESS

Demonstration of a spherical plasma mirror for the counter-propagating kilojoule-class petawatt LFEX laser system

SADAOKI KOJIMA,[1,*] YUKI ABE,[2,3] EISUKE MIURA,[4] TETSUO OZAKI,[5] KOHEI YAMANOI,[3] TOMOKAZU IKEDA,[3] YUBO WANG,[3] JINYUAN DUN,[3] SHUWANG GUO,[3] TAMAKI MAEKAWA,[3] RYUNOSUKE TAKIZAWA,[3] HIROKI MORITA,[3] SHOUI ASANO,[3] YASUNOBU ARIKAWA,[3] HIROSHI SAWADA,[6] KATSUHIRO ISHII,[7] RYOHEI HANAYAMA,[7] SHINICHIRO OKIHARA,[7] YONEYOSHI KITAGAWA,[7] YASUHIRO KAJIMURA,[8] ALESSIO MORACE,[3] HIROYUKI SHIRAGA,[3] KEISUKE SHIGEMORI,[3] ATSUSHI SUNAHARA,[3,9] NATSUMI IWATA,[3,10] TAKAYOSHI SANO,[3] YASUHIKO SENTOKU,[3] TOMOYUKI JOHZAKI,[3,11] MASAHARU NISHIKINO,[1] AKIFUMI IWAMOTO,[3,5] KENICHI NAGAOKA,[5] HITOSHI SAKAGAMI,[5] SHINSUKE FUJIOKA,[3] AND YOSHITAKA MORI[7]

[1] *Kansai Photon Science Institute, National Institutes for Quantum and Radiological Science and Technology, 8-1-7 Umemidai, Kizugawa, Kyoto 619-0215, Japan*
[2] *Graduate School of Engineering, Osaka University, 2-1 Yamadaoka, Suita, Osaka 565-0871, Japan*
[3] *Insititute of Laser Engineering, Osaka University, 2-6 Yamada-oka, Suita, Osaka 565-0871, Japan*
[4] *National Institute of Advanced Industrial Science and Technology, 1-1-1 Umezono, Tsukuba, Ibaraki 305-8568, Japan*
[5] *National Institute for Fusion Science, 322-6 Oroshi-cho, Toki, Gifu 509-5292, Japan*
[6] *Department of Physics, University of Nevada Reno, Reno, NV 89557, USA*
[7] *The Graduate School for the Creation of New Photonics Industries, 1955-1 Kurematsu-cho, Hamamatsu, Shizuoka 431-1202, Japan*
[8] *National Institute of Technology, Akashi College, 679-3 Nishioka, Uozumi-cho, Akashi, Hyogo 674-8501, Japan*
[9] *Center for Materials under Extreme Environments, School of Nuclear Engineering, Purdue University, 500 Central Drive, West Lafayette, IN 47907, USA*
[10] *Institute for Advanced Co-Creation Studies, Osaka University, 1-1 Yamadaoka, Suita, Osaka 565-0871, Japan*
[11] *Graduate School of Advanced Science and Engineering, Hiroshima University, 1-4-1 Kagamiyama, Higashi-Hiroshima, Hiroshima 739-8527, Japan*
[*] *kojima.sadaoki@qst.go.jp*

Abstract: A counter-propagating laser-beam platform using a spherical plasma mirror was developed for the kilojoule-class petawatt LFEX laser. The temporal and spatial overlaps of the incoming and redirected beams were measured with an optical interferometer and an x-ray pinhole camera. The plasma mirror performance was evaluated by measuring fast electrons, ions, and neutrons generated in the counter-propagating laser interaction with a Cu-doped deuterated film on both sides. The reflectivity and peak intensity were estimated as ~50% and $\sim 5 \times 10^{18}$ W/cm^2, respectively. The platform could enable studies of counter-streaming charged particles in high-energy-density plasmas for fundamental and inertial confinement fusion research.

#475945 https://doi.org/10.1364/OE.475945
Journal © 2022 Received 4 Oct 2022; revised 28 Oct 2022; accepted 28 Oct 2022; published 10 Nov 2022

Optics EXPRESS

1. Introduction

A plasma mirror is a vital optical component in high-intensity, short-pulse laser experiments to enhance the temporal contrast of an ultra-intense pulse for controlling the laser-target interaction conditions. A thin plasma layer produced on the surface of a laser-irradiated solid acts as a light reflector for a picosecond duration. Since the demonstration [1,2] and characterization [3,4] of plasma mirrors using a flat substrate, this technique has been widely used to suppress prepulse and amplified spontaneous emission to improve the contrast from the pedestal to the main pulse to be on the order of 10^9 to $\sim 10^{11}$ [5–8]. In addition, an elliptical plasma mirror substrate has been demonstrated to realize an extremely short focal length with an intensity beyond 10^{20} W/cm^2 [9,10].

The use of a plasma mirror as a beam redirecting [11] and focusing tool enables a single bundle of laser beams for one-sided irradiation to be transformed into a counter-propagating laser system. This laser configuration could be a new experimental platform to study various physics involved in counter laser-irradiation, laser-driven particle interactions, and the collision of the beam with background plasmas. For example, two counter-propagating flows of fast electrons in an overdense plasma generate mega-Gauss magnetic filaments through two-stream Weibel instabilities [12,13], which could be a key physical mechanism for enhancing the electron energy coupling to the background plasma for heating a compressed fusion fuel together with beam-induced plasma waves [14]. In a magnetized plasma, thermonuclear fusion reactions could be triggered by collapsing standing whistler waves excited by crossing intense laser beams [15,16]. In addition, counter laser irradiation on a structured target with intensities beyond 10^{22} W/cm^2 gives high-density gamma-rays, producing positrons through the linear Breit-Wheeler process that has not yet been observed [17]. So far, a joule-class, high-intensity counter-propagating laser system has been built and demonstrated for fast ignition experiments [12,13], and kilojoule-class counter-two-beam experiments have been proposed [18]. However, because of the substantial risk of configuring high-peak-power laser pulses in such a geometry and the high costs and time required for modifying existing high-energy beams with large optics, counter-propagating relativistic intensity laser experiments have not been performed until now.

Here, we report the development and demonstration of a spherical concave plasma mirror for the kilojoule-class petawatt LFEX laser to achieve counter beam configuration. In our previous studies, we focused on the contrast-enhancing effect of plasma mirrors. Here, we focus on the beam-redirecting effect of plasma mirrors. The LFEX laser system at the Institute of Laser Engineering, Osaka University delivers four beams with a total of 1.6 kJ in a picosecond-duration pulse [19]. A counter-propagating geometry was achieved for the first time by redirecting and focusing two beams with a spherical plasma mirror, while the others were focused with an off-axis parabolic (OAP) mirror. The advantage of using plasma mirrors as optics for redirection is that they can handle high-fluence laser beams of over 50 J/cm^2, and thus can redirect a 1600 J laser beam with a mirror only 2 in. (1 in. = 2.54 cm) in diameter. In contrast, a spherical mirror with a diameter of about 1 m would need to be placed 4 m from the focal point to avoid damage to the mirror surface. Although the plasma mirror must be replaced after each laser shot, it is an attractive approach for counter-irradiation studies of kilojoule-class lasers at low cost and without modifications to existing facilities. Because the current shot rate for Nd:glass-based lasers is about once every 1 or 2 h, the plasma mirror can be replaced between shots.

A focal spot degradation by the spherical plasma mirror was evaluated using an off-line alignment system and ray-tracing calculations. The temporal and spatial overlaps of the counter-propagating pulses were measured in the vacuum chamber with an optical interferometer and x-ray pinhole imaging. Finally, with high-energy LFEX beams, irradiation of the counter-propagating relativistic laser pulses on a Cu-doped deuterated target from both sides was demonstrated.

Optics EXPRESS

2. Design of the spherical concave plasma mirror for beam redirecting and focusing

A spherical concave plasma mirror was designed to reflect and focus two LFEX beams irradiating on one side of a planar target, while the other two were focused with an OAP mirror. Figure 1(a) shows a schematic of the counter-propagating LFEX laser configuration with a spherical plasma mirror. The plasma mirror was initially designed for four LFEX beams [Fig. 1(b)] with a total energy of 1.6 kJ and has been demonstrated to produce ultra-high contrast pulses with reflectivity of 50% and laser fluence of 50–100 J/cm^2 [8]. In the present work, a 2-in. concave mirror with a radius of curvature of 202 mm (f = 101 mm) was chosen, as used in the previous experiments. In the counter laser illumination operation, the path of the two beams [beams 2 and 4, shown in red in Fig. 1(a)] for the redirection of the beams was offset to 3 mm above the target chamber center (TCC), whereas beams 1 and 3 [shown in blue in Fig. 1(a)] were directly focused at the TCC by an f/10 OAP mirror. The 3 mm offset was a maximum distance due to limitations in the observation field of view of the laser spot monitor. Each beam used half a mirror segment to produce plasma on a clean surface.

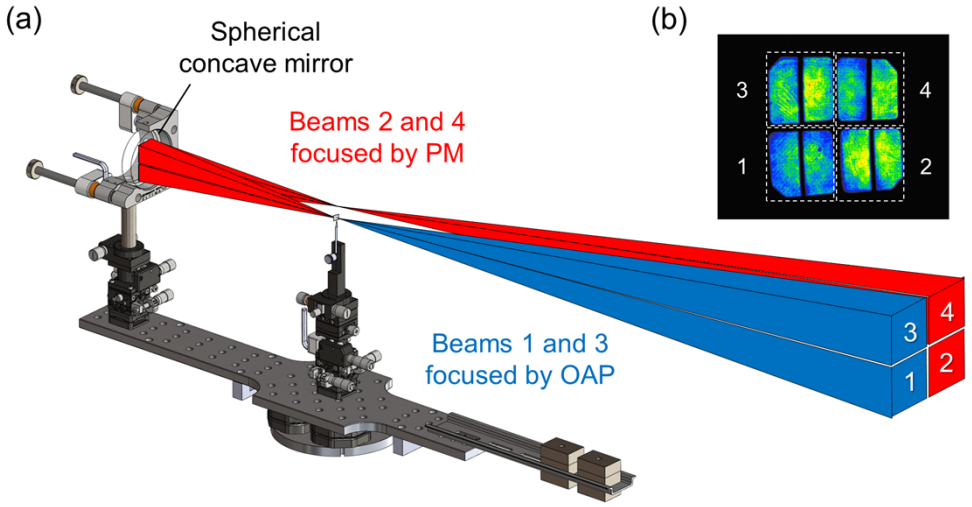

Fig. 1. (a) Schematic of the counter laser irradiation configuration with a spherical plasma mirror for the kilojoule-class petawatt LFEX laser system. (b) Near-field beam pattern of the LFEX laser on the OAP mirror.

An aberrated focal spot image formed by the tilted spherical mirror was evaluated by ray-tracing calculations. Assuming an infinitesimally small point source, changes in focal spot images and Strehl ratio were calculated as a function of the offset distance using the OpTaliX-Pro code (ver.8.70) [20]. Strehl ratio is defined as the ratio of the intensity peak of an unaberrated to an aberrated spot profile [21]. Figure 2(a) shows the ray diagram of a ray-tracing calculation for a spherical concave mirror. The focal point of the spherical mirror on the optic axis denoted as the first imaging point, was imaged to a vertically offset position by a distance of d (the second imaging point).

Ray-tracing calculations were performed for two near-field laser beam patterns on a plasma mirror. The first case was a top-hat round beam (40 mm diameter), which assumed a He-Ne laser in a pre-alignment system [Fig. 2(b)]. The second was a top-hat rectangular beam (20×40 mm), which assumed two vertically aligned LFEX beams (beams 2 and 4), conditions similar to the actual LFEX shots [Fig. 2(c)]. Figure 2(d) shows the result of calculated Strehl ratios as a function of the separation distance for two near-field beam patterns. At a separation distance of 3

Optics EXPRESS

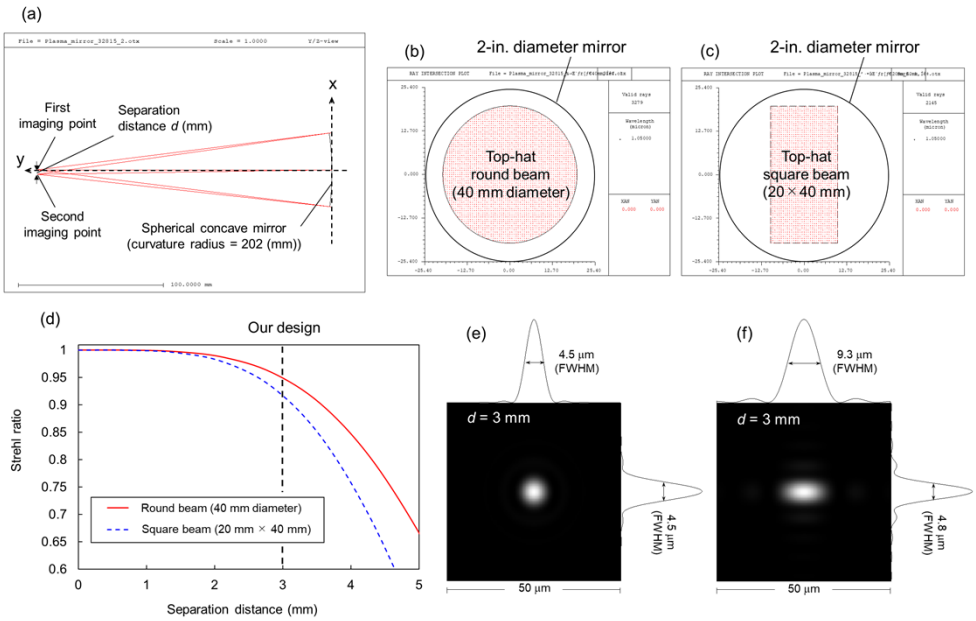

Fig. 2. (a) Ray diagram for the ray-tracing calculations for the spherical concave mirror. (b) Near-field pattern (NFP) of the top-hat round beam. (c) NFP of the top-hat rectangular beam. (d) Calculated Strehl ratios as a function of the separation distance. (e) Far-field pattern (FFP) at the second imaging point with separation distance $d = 3$ mm for the top-hat round beam. (f) FFP for the top-hat rectangular beam.

mm, the Strehl ratio remained 0.95 for the round beam (red solid line) and 0.92 for the rectangular beam (blue dashed line). The far-field spot was calculated to be 4.5 μm in the full width at half maximum (FWHM) for the round beam and it was symmetrical horizontally and vertically [Fig. 2(e)]. However, the rectangular beam had different spot diameters in the horizontal and vertical directions due to the different F values. The far spot was calculated to be 9.3 μm (FWHM) in the horizontal direction and 4.8 μm (FWHM) in the vertical direction [Fig. 2(f)]. These spot size distortions are acceptable, especially for the 50 μm (FWHM) spot of the LFEX laser beams. An off-line spot size measurement was performed to verify this calculated result, as shown in Sec. 3.

3. Off-line alignment system and focal spot measurement

The alignment of the plasma mirrors to the TCC and the focal spot measurement were performed on a pre-alignment system built outside the Gekko-XII vacuum chamber for high-energy LFEX laser experiments. As shown in Fig. 3(a), the system consisted of two orthogonally configured low-magnification (×10) cameras for target positioning and one high-magnification (×50) camera for focal spot measurement. In addition, a He-Ne laser was set to define the path of the LFEX alignment laser axis with the same f-number as the LFEX laser. The plasma mirror and a laser target were mounted on a breadboard (top board) with a magnetic base, which was then attached to the bottom board, as shown in Fig. 3(b). A planar foil with two 100 μm diameter pinholes separated by 3 mm vertically was used to fix the relative position of the three points: the first imaging point, the mirror surface, and the second imaging point at the TCC. The He-Ne laser passing through the upper pinhole was reflected at the center of the mirror and then sent back through the lower pinhole at the TCC by adjusting the tip and tilt of the mirror. For focal spot

Optics EXPRESS

measurements, a small flat mirror was set at the TCC to reflect the alignment beam to the spot monitor. Finally, the focal spot diameter was optimized by adjusting the spherical mirror while keeping the beam pointing the same way. After completing the off-line plasma mirror and target alignment, the top board with the double pinhole substrate was transferred to the bottom board stage. The mirror position and focus were also confirmed with the LFEX alignment laser inside the vacuum chamber.

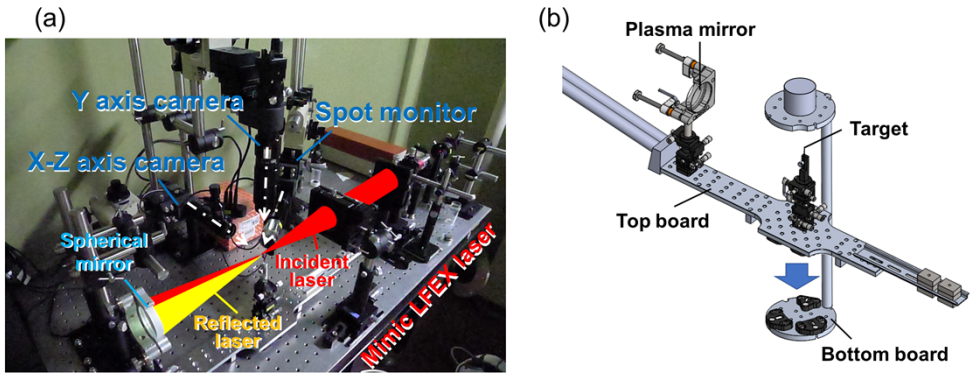

Fig. 3. (a) Pre-alignment system configured with the two orthogonally aligned low-magnification (×10) cameras to monitor the target position, one high-magnification (×50) camera to measure the laser focal spot size, and a He-Ne laser focused by a lens with the same f-number as the LFEX laser system. (b) Schematic of the plasma mirror and target mounted on the top board. The entire board was placed on the bottom board and lowered into the vacuum target chamber center for the final alignment and high-energy laser shots.

The quality of the beam profiles formed by the focusing lens and the spherical plasma mirror were compared by using the He-Ne laser source on the off-line alignment system. Figure 4(a) and 4(b) show measurements of the spot images of the He-Ne laser beam at the first and second imaging points. The incoming beam was focused by a plano-convex lens to a 13 μm spot diameter (FWHM) at the first imaging point, and the second focused by the spherical concave mirror had a 16 μm spot size. The broadening of the focal spot profile caused by the spherical mirror was estimated as $(16\ \mu m^2 - 13\ \mu m^2)^{1/2} = 9.3\ \mu m$ [Fig. 4(c)]. In other words, the broadened profile resulted from a convolution of the original profile with a 9.3 μm FWHM gaussian function. In comparison, the focal spot image of the LFEX laser shown in Fig. 4(d) had an FWHM of ~50 μm. The 50 μm diameter LFEX beam profile convolved with the Gaussian function gave a 50.8 μm diameter spot. Therefore, the distortion of the large focal spot by the spherical mirror due to the 3 mm offset was negligible.

Optics EXPRESS

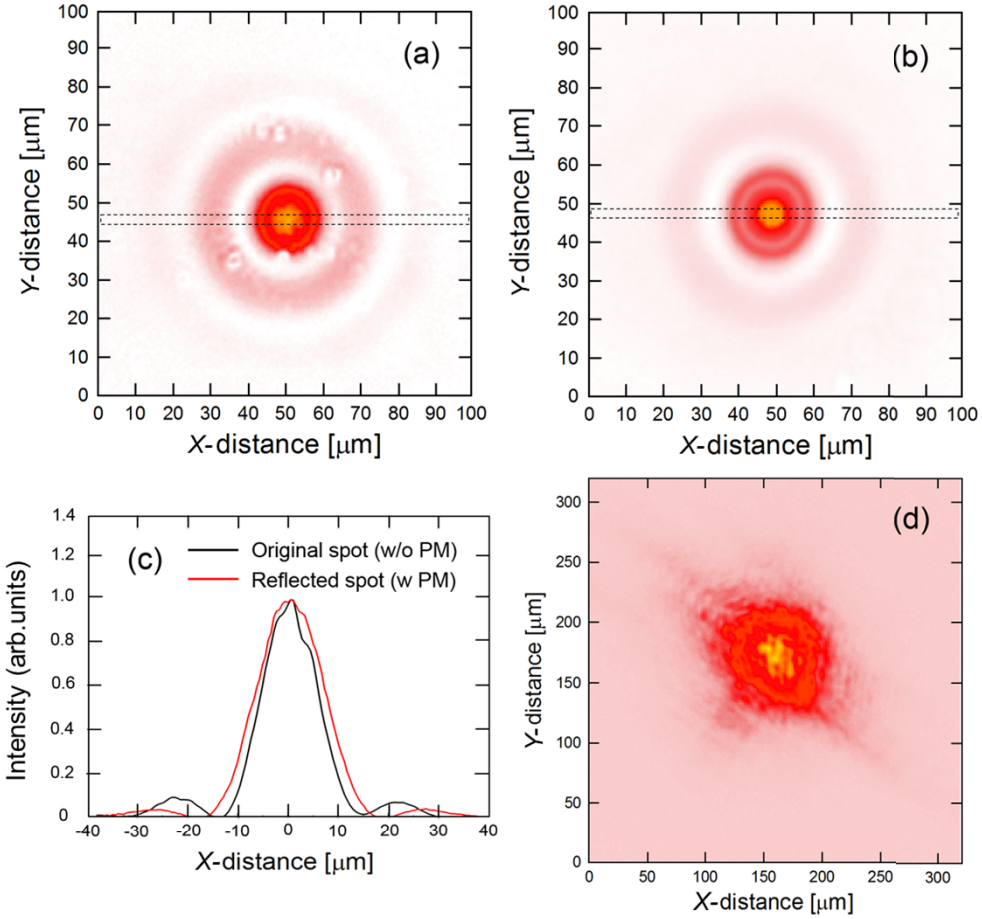

Fig. 4. (a) Original spot image of the He-Ne laser at the first imaging point. (b) Spot image relayed by the spherical concave mirror at the second imaging point. (c) Comparison of the focal spot profiles. (d) Measured LFEX beam spot.

4. Measurement of the temporal beam overlap

The extra beam path for the two LFEX beams redirected by the plasma mirror requires the addition of a timing delay for co-timed counter laser irradiation on both sides of a planar target at the TCC. The temporal overlap of the counter-propagating LFEX beams [see Fig. 1] was measured by an optical interferometer using 6 Hz, 10 mJ pre-amplified LFEX pulses. To form interference fringes with the temporally overlapping beams, an aluminum-coated, right-angled prism was placed at the TCC to reflect both beams focused by the OAP and spherical plasma mirror. The reflected beams diverged as they propagated outside the vacuum chamber, and the beams overlapped well, forming interference fringes at a CCD detector plane when co-timed. The initial timing of the beams redirected by the plasma mirrors (beams 2 and 4) was set 1.35 ns earlier than the others to compensate for the path difference. As described in Sec. 3, the spatial overlap of the counter-propagating beams was ensured using the double pinhole target and the LFEX alignment laser.

Figure 5(a) shows the interference fringe measurement of a timing delay scan. The fringe patterns were clearly observed during delays between 58 and 60 ps. The frequency component of the fringe data was analyzed, and its intensity is plotted as a function of time in Fig. 5(b). It

Optics EXPRESS

followed a nearly Gaussian temporal profile peaking at 59 ps with a width of 2.6 ps (FWHM). The relationship between the width of the autocorrelation and that of the original pulse can be described by $\Delta\tau_{Auto}^{FWHM} = 1.41\Delta\tau_{original}^{FWHM}$. Based on the width of 1.9 ps (FWHM) of the original pulse, this result is consistent with the pulse duration observed by the single-shot autocorrelator using the second harmonic generation. The measurement of the interference fringes demonstrated the temporal synchronization of the kilojoule-class petawatt laser pulses for the counter-propagating laser configuration within the accuracy of the pulse duration.

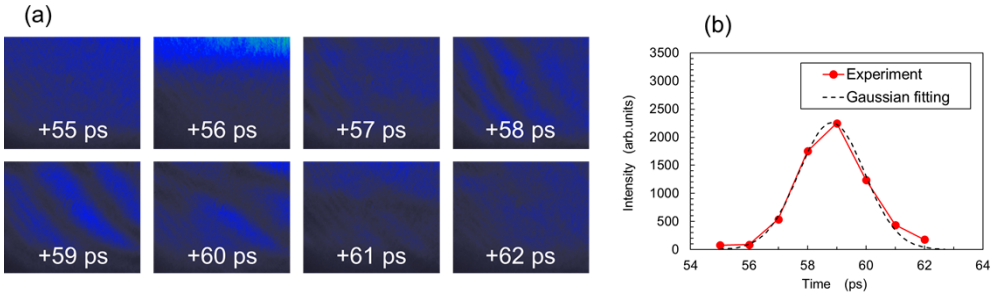

Fig. 5. (a) Measurements of interference fringes for various relative timing delays between the beams focused by the plasma mirror and OAP. (b) Temporal variation in the fringe intensity. The measured intensity profile was fitted with a Gaussian function, indicating the maximum timing was at 59 ps and the width was 2.6 ps (FWHM).

5. Experiment with the high-energy LFEX beams

5.1. Experimental conditions

The performance of the spherical plasma mirror, such as the spatial beam overlap at the target plane, the mirror reflectivity, and the on-target intensity, was evaluated in a counter-propagating laser experiment conducted with high-energy LFEX beams. The energy of the LFEX beams was set to 300 J/beam on the plasma mirror side and 150 J/beam on the OAP side. In Ref. [8], Fig. 2(b) shows the reflectivity as a function of laser fluence. At 20 J/cm^2, the lowest fluence in the data series, the reflectivity was 8%, but it quickly increased above 30 J/cm^2 to about 50%. At even higher fluences, the reflectance decreased slowly and approached about 35% when the fluence exceeded 1000 J/cm^2. Therefore, in the present work, the laser energy was chosen so that the lowest fluence in the entire beam was not less than 30 J/cm^2 to obtain good reflectivity across the entire reflective pattern. The pulse duration was measured to be 1.3–2.1 ps, and the accuracy of the temporal beam overlap was better than 1.9 ps. An off-line focal spot measurement of the LFEX alignment laser indicated that 80% of the beam energy was encircled within a 70 μm diameter spot.

The interaction of the high-energy, short-pulse beams with a planar target on both sides was diagnosed by measuring x-rays, charged particles, and neutron signals as a signature of relativistic laser-matter interaction. A Cu-doped deuteride polystyrene film [22] was developed for simultaneous measurements of characteristic x-rays and neutrons produced in beam-beam fusion reactions. The atomic concentration of the Cu dopant in the 10-μm-thick film was approximately 13.5 wt %. Figure 6 shows a schematic of the diagnostics layout. An x-ray pinhole camera [23] was fielded at 52.6° from the laser axis. Image plate-based magnetic electron-ion spectrometers [24] were installed downstream of the laser axes on each side (ESM1 in p47 and ESM2 in p48). In addition, the multi-channel neutron time-of-flight detector [25] was placed at 54.7° from the laser axis and 13.5 m from the target to observe spectral modulation of neutrons from the deuterium-deuterium (DD) reaction. As discussed in the following sections, x-ray pinhole images

Optics EXPRESS

were used to evaluate the spatial overlap of the counter-propagating beams in Sec. 5.2, and the reflectivity of the plasma mirror was inferred by comparing the number and spectrum of fast electrons on each side in Sec. 5.3. The neutron spectrum is also discussed in Sec. 5.3 to clarify the acceleration of deuterons and their interaction with bulk nuclei in the target.

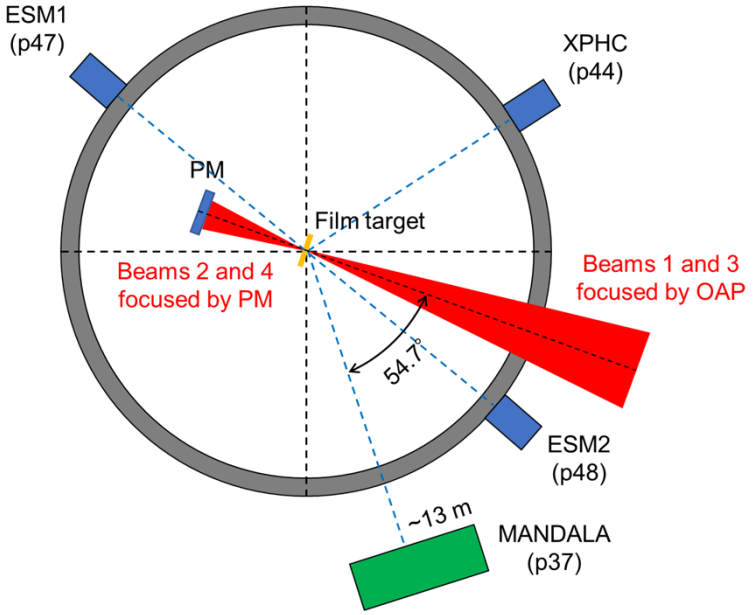

Fig. 6. Schematic of the plasma mirror (PM), the LFEX beams, and diagnostics, including an x-ray pinhole camera (XPHC), electron energy spectrometers (ESM1 and ESM2), and a multi-channel time-of-flight neutron spectrometer (MANDALA).

5.2. Evaluation of plasma mirror performance

X-ray pinhole camera images provided information on the spatial overlap of the counter-propagating beams and on-target laser intensity on each side. Two similar target shots (L4415 and L4411) were examined, in which the beam energies on the plasma mirror and OAP were 403 and 756 J for shot L4415, and 311 and 600 J for shot L4411, respectively. Figure 7(a) is a layout of the film target with the counter propagating beams from the camera's line of sight. Two distinct x-ray emission spots were observed on L4415 [Fig. 7(b)]. The two spots were produced by the beams focused by the OAP mirror (beams 1 and 3) and plasma mirror (beams 2 and 4). The shape of the x-ray emission spots was approximately elliptical, suggesting that the major axis of the x-ray spot could be related to the beam spot diameter. In this shot, the major spot diameters of beams 1 and 3 were estimated to be 50 μm, and those of beams 2 and 4 were estimated to be 56 μm (FWHM). The spot diameters were similar and nearly equal to the measured spot size of the alignment laser of 70 μm. The result suggested that the mirror's aberration was insignificant in focusing the large diameter beams, as described in Sec. 3.

Furthermore, the reflectivity of the plasma mirror was evaluated from the intensity of the x-ray emission in the images. The pinhole camera had a 50-μm-thick Be filter and an imaging plate detector (BAS-SR, Fujifilm), transmitting x-rays above 2 keV [23]. In this x-ray range, a dominant x-ray source is thermal plasma, where the x-ray intensity is proportional to the electron temperature of the hot plasma produced by the intense picosecond pulses irradiating the target surface. Figure 7(d) shows the line profiles along the minor axis of the x-ray spots after subtracting the image background. In L4415, the peak intensities of the spots of beams 1 and

Optics EXPRESS

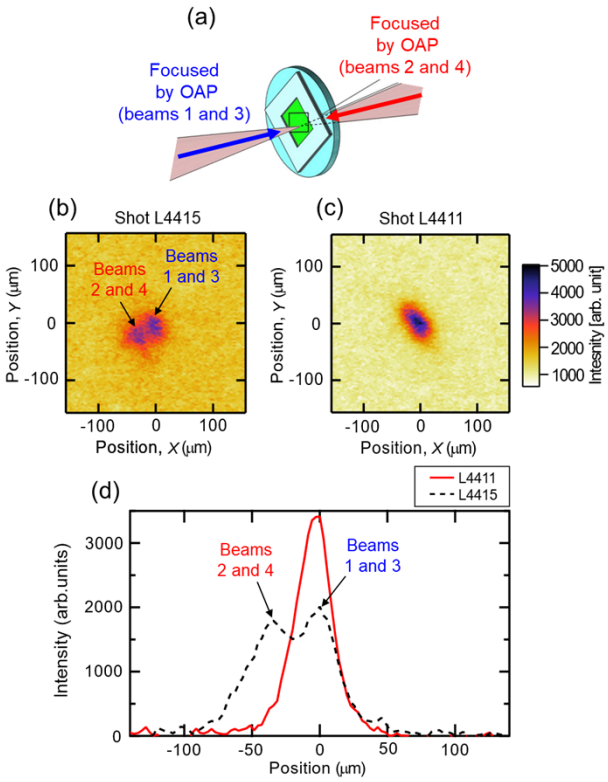

Fig. 7. (a) Schematic of a Cu-doped deuteride polystyrene film with the counter-propagating laser beams from the view of the x-ray pinhole camera. Pinhole camera images of the x-ray emissions on (b) shot L4415 and (c) shot L4411. In (b), the emission spots denoted as beams 1 and 3, and beams 2 and 4 were produced by the beams from the OAP and plasma mirror, respectively. (d) Intensity profile along the minor axis of the x-ray emissions. The profile for shot L4411 is the solid red line and that for shot L4415 is the dashed black line.

3, and beams 2 and 4 were comparable (intensity ratio of 1.12), whereas the x-ray intensity for L4411 was about twice that of each peak in shot L4415. From the x-ray intensity of the pinhole camera images and the laser energy ratio, the reflectivity of the plasma mirror was estimated to be 48%, which was consistent with the expected reflectivity [8]. Based on the estimated reflectivity, the on-target intensity was calculated to be 5×10^{18} W/cm^2 per side on the surface of the Cu-doped deuteride polystyrene film.

5.3. *Demonstration of fast electron and ion acceleration by the counter-propagating relativistic intensity pulses*

The interaction of the counter-propagating high-energy LFEX beams with the Cu-doped deuteride foil was examined by measuring laser-accelerated relativistic electrons and neutron spectra produced in the beam-target fusion reaction. Figure 8(a) shows the time-integrated energy distribution of escaped fast (hot) electrons generated by the LFEX beams focused with OAP on ESM 1 (red dots) and the plasma mirror on ESM 2 (blue triangles). Because the relativistic laser-target interaction accelerates the highest-energy electrons downstream of the laser injection axis, the order of the on-target peak laser intensity can be deduced by comparing the slope of a measured electron spectrum with an intensity-dependent scaling law. The measured spectrum fitted with a single slope temperature, T_{hot}, of a Maxwell distribution function [$f(E) \sim \exp(-E/T_{\mathrm{hot}})$] identified

Optics EXPRESS

T_{hot} of 0.58 MeV for the beams focused by OAP and T_{hot} of 0.65 MeV for the beams focused by the plasma mirror. Considering the use of the plasma mirror and the contrast-improved LFEX pulses, we used a ponderomotive scaling law, which is given by $T_{hot} = 0.511\left(\sqrt{1+\frac{I\lambda^2}{2.8\times10^{18}}}-1\right)$ MeV [26], where I_L is the laser intensity in watts per square centimeter and λ_L is the laser wavelength in micrometers. From the scaling law and measurements, peak laser intensities of 4.5×10^{18} and 5.3×10^{18} W/cm^2 were estimated for the OAP and the plasma mirror sides, respectively. These intensities corresponded to the values of 5×10^{18} W/cm^2 calculated from the measured laser energy, pulse duration, and focal spot size. In addition, the energy on the plasma mirror side was pre-set to about twice that on the OAP side to compensate for the reflectivity of about 50%. The electron measurement in Fig. 8(a) shows that the slope temperature of electrons generated was comparable in ESM1 and ESM2, supporting the reflectivity of the plasma mirror of ~50%.

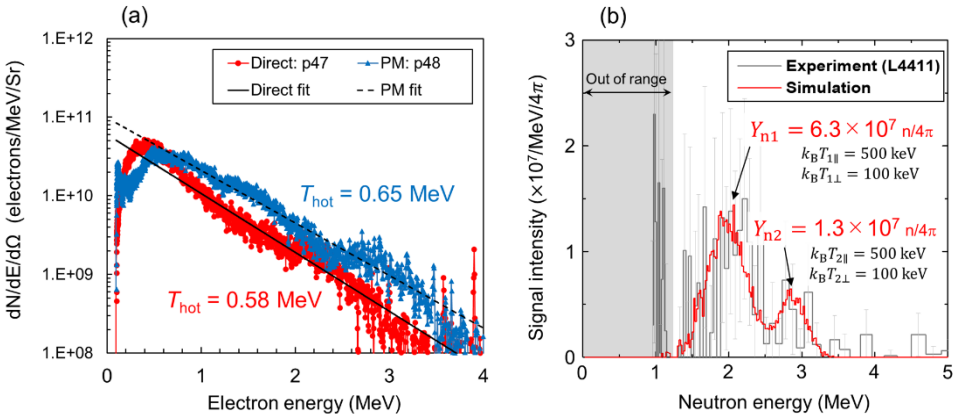

Fig. 8. (a) Hot electron energy spectra observed in the directions of the plasma mirror and OAP and (b) measured DD-neutron spectrum for shot L4411.

The successful operation of the plasma mirror on shot L4411 resulted in effective ion acceleration on both sides of the target foil. The ion acceleration produced a counter stream of non-thermal deuterons interacting with bulk nuclei in the target. The resulting DD reactions produced neutrons with a characteristic spectrum [Fig. 8(b)]. The measured neutrons were split into two spectral components yielding 6.3×10^7 and 1.3×10^7 n/shot. The spectral shape was the result of a strong Doppler effect caused by the reacting particles. Deuterons coming toward the detector produced neutrons with energies higher than 2.45 MeV, whereas deuterons moving away from the detector produced neutrons with energies less than 2.45 MeV. Therefore, the measured double-peaked neutron spectrum indicated the presence of deuterons traveling to and from the target in the opposite directions. The spectral shape was consistent with the calculated results [red curve in Fig. 8(b)], obtained by using Monte Carlo code based on the two-body collision model [27]. The code simulated DD reactions between bulk deuterium atoms ($v_d = 0$) and nonthermal deuterons with an anisotropic Maxwellian distribution of $f_d = \exp(-0.5m_d(v_{d\parallel}^2/k_BT_\parallel + v_{d\perp}^2/k_BT_\perp))$, where m_d is deuteron mass, k_B is the Boltzmann constant, and $T_\parallel$ and $T_\perp$ are the temperatures in the longitudinal and lateral directions with respect to the laser axis. The estimated deuteron temperatures were $k_BT_\parallel$ = 500 keV and $k_BT_\perp$ = 100 keV for both spectral components, indicating strong directionality of the deuteron beams. These results also showed that the laser focal spots on both sides reached relativistic intensities (>10^{18} W/cm^2) and produced megaelectron volt-scale ion counter stream propagating on the target.

Optics EXPRESS

6. Conclusions

The counter-propagating laser platform using a spherical plasma mirror for the kilojoule-class petawatt LFEX laser system was demonstrated. An off-line alignment system allowed us to establish the positioning and focusing of the plasma mirror on the TCC. In addition, the focal spot image measured by using a He-Ne laser and ray-tracing calculations showed the effects of aberration from the spherical mirror to be minimal, especially for a 50 μm diameter LFEX laser spot. The timing synchronization accuracy between the counter-propagating pulses was estimated to be within 1.9 ps in the optical interference measurements. X-ray pinhole camera images confirmed the spatial overlap of the counter-propagating laser beams with a spot size of ~60 μm. In the high-energy LFEX experiment, the counter-propagating beams were focused on the Cu-doped deuteride polystyrene film. The direct LFEX beams and beams redirected by the plasma mirror produced a similar number of fast electrons and slope temperature in the fast electron energy distributions. The measurement with the ponderomotive scaling law indicated that the peak on-target intensity of 5×10^{18} W/cm^2 per side was achieved. Furthermore, the double-peak spectrum in the neutron measurement suggested that each counter-propagating beam accelerated fast deuterons. The experiment demonstrated the operation of the spherical plasma mirror with the high-energy picosecond LFEX beams. The generation of laser-driven high-energy charged particles and neutrons is promising for promoting the counter-propagating laser platform for studies of counter-streaming quantum beams, innovative heating schemes for inertial confinement fusion, and fundamental research for quantum electrodynamics.

Funding. National Institute for Fusion Science (NIFS20KUGK132); Institute of Laser Engineering at Osaka University (2020B2-010, 2021B2-022, 2022B2-022); Ministry of Education, Culture, Sports, Science and Technology (22K14021, JPMXS0450300021, 19H01870).

Acknowledgments. We thank the technical support staff of the Institute of Laser Engineering (ILE) at Osaka University, and those of the Plasma Simulator at the National Institute for Fusion Science (NIFS) for assistance with laser operation, target fabrication, plasma diagnostics, and computer simulations. We also acknowledge the FIREX-I advisory board member, K. A. Tanaka, S. P. Regan, H. Yoneda, Y. Fukuda, and H. Yamada for useful discussions.

Disclosures. The authors declare no conflicts of interest.

Data availability. Data underlying the results presented in this paper are not publicly available at this time but may be obtained from the authors upon reasonable request.

References

1. H. C. Kapteyn, M. M. Murnane, A. Szoke, and R. W. Falcone, "Prepulse energy suppression for high-energy ultrashort pulses using self-induced plasma shuttering," Opt. Lett. **16**(7), 490–492 (1991).
2. D. M. Gold, "Direct measurement of prepulse suppression by use of a plasma shutter," Opt. Lett. **19**(23), 2006–2008 (1994).
3. B. Dromey, S. Kar, M. Zepf, and P. Foster, "The plasma mirror—A subpicosecond optical switch for ultrahigh power lasers," Rev. Sci. Instrum. **75**(3), 645–649 (2004).
4. G. Doumy, F. Quéré, O. Gobert, M. Perdrix, P. Martin, P. Audebert, J. C. Gauthier, J.-P. Geindre, and T. Wittmann, "Complete characterization of a plasma mirror for the production of high-contrast ultraintense laser pulses," Phys. Rev. E **69**(2), 026402 (2004).
5. A. Lévy, T. Ceccotti, P. D'Oliveira, F. Réau, M. Perdrix, F. Quéré, P. Monot, M. Bougeard, H. Lagadec, P. Martin, J.-P. Geindre, and P. Audebert, "Double plasma mirror for ultrahigh temporal contrast ultraintense laser pulses," Opt. Lett. **32**(3), 310–312 (2007).
6. S. Inoue, K. Maeda, S. Tokita, K. Mori, K. Teramoto, M. Hashida, and S. Sakabe, "Single plasma mirror providing 10^4 contrast enhancement and 70% reflectivity for intense femtosecond lasers," Appl. Opt. **55**(21), 5647–5651 (2016).
7. I. W. Choi, C. Jeon, S. G. Lee, S. Y. Kim, T. Y. Kim, I. J. Kim, H. W. Lee, J. W. Yoon, J. H. Sung, S. K. Lee, and C. H. Nam, "Highly efficient double plasma mirror producing ultrahigh-contrast multi-petawatt laser pulses," Opt. Lett. **45**(23), 6342–6345 (2020).
8. Y. Arikawa, S. Kojima, A. Morace, S. Sakata, T. Gawa, Y. Taguchi, Y. Abe, Z. Zhang, X. Vaisseau, S. H. Lee, K. Matsuo, S. Tosaki, M. Hata, K. Kawabata, Y. Kawakami, M. Ishida, K. Tsuji, S. Matsuo, N. Morio, T. Kawasaki, S. Tokita, Y. Nakata, T. Jitsuno, N. Miyanaga, J. Kawanaka, H. Nagatomo, A. Yogo, M. Nakai, H. Nishimura, H. Shiraga, S. Fujioka, F. Group, L. Group, H. Azechi, A. Sunahara, T. Johzaki, T. Ozaki, H. Sakagami, A. Sagisaka, K. Ogura, A. S. Pirozhkov, M. Nishikino, K. Kondo, S. Inoue, K. Teramoto, M. Hashida, and S. Sakabe, "Ultrahigh-contrast kilojoule-class petawatt LFEX laser using a plasma mirror," Appl. Opt. **55**(25), 6850–6857 (2016).

Optics EXPRESS

9. M. Nakatsutsumi, A. Kon, S. Buffechoux, P. Audebert, J. Fuchs, and R. Kodama, "Fast focusing of short-pulse lasers by innovative plasma optics toward extreme intensity," Opt. Lett. **35**(13), 2314–2316 (2010).
10. R. Wilson, M. King, R. J. Gray, D. C. Carroll, R. J. Dance, N. M. H. Butler, C. Armstrong, S. J. Hawkes, R. J. Clarke, D. J. Robertson, C. Bourgenot, D. Neely, and P. McKenna, "Development of focusing plasma mirrors for ultraintense laser-driven particle and radiation sources," Quantum Beam Sci. **2**(1), 1 (2018).
11. G. G. Scott, D. A. Mariscal, D. Canning, R. F. Heeter, M. Krieger, R. J. Wallace, C. McGuffey, J. L. Peebles, R. A. Simpson, C. Stoeckl, and T. Ma, "Demonstration of plasma mirror capability for the OMEGA Extended Performance laser system," Rev. Sci. Instrum. **93**(4), 043006 (2022).
12. Y. Mori, Y. Nishimura, R. Hanayama, S. Nakayama, K. Ishii, Y. Kitagawa, T. Sekine, N. Sato, T. Kurita, T. Kawashima, H. Kan, O. Komeda, T. Nishi, H. Azuma, T. Hioki, T. Motohiro, A. Sunahara, Y. Sentoku, and E. Miura, "Fast heating of imploded core with counterbeam configuration," Phys. Rev. Lett. **117**(5), 055001 (2016).
13. Y. Mori, Y. Nishimura, R. Hanayama, S. Nakayama, K. Ishii, Y. Kitagawa, T. Sekine, Y. Takeuchi, T. Kurita, N. Satoh, T. Kawashima, O. Komeda, T. Nishi, H. Azuma, T. Hioki, T. Motohiro, A. Sunahara, Y. Sentoku, and E. Miura, "Fast heating of fuel assembled in a spherical deuterated polystyrene shell target by counter-irradiating tailored laser pulses delivered by a HAMA 1 Hz ICF driver," Nucl. Fusion **57**(11), 116031 (2017).
14. N. Ratan, N. J. Sircombe, L. Ceurvorst, J. Sadler, M. F. Kasim, J. Holloway, M. C. Levy, R. Trines, R. Bingham, and P. A. Norreys, "Dense plasma heating by crossing relativistic electron beams," Phys. Rev. E **95**(1), 013211 (2017).
15. T. Sano, Y. Tanaka, N. Iwata, M. Hata, K. Mima, M. Murakami, and Y. Sentoku, "Broadening of cyclotron resonance conditions in the relativistic interaction of an intense laser with overdense plasmas," Phys. Rev. E **96**(4), 043209 (2017).
16. T. Sano, S. Fujioka, Y. Mori, K. Mima, and Y. Sentoku, "Thermonuclear fusion triggered by collapsing standing whistler waves in magnetized overdense plasmas," Phys. Rev. E **101**(1), 013206 (2020).
17. Y. He, T. G. Blackburn, T. Toncian, and A. V. Arefiev, "Dominance of γ-γ electron-positron pair creation in a plasma driven by high-intensity lasers," Commun. Phys. **4**(1), 139 (2021).
18. J. Zhang, W. M. Wang, X. H. Yang, D. Wu, Y. Y. Ma, J. L. Jiao, Z. Zhang, F. Y. Wu, X. H. Yuan, Y. T. Li, and J. Q. Zhu, "Double-cone ignition scheme for inertial confinement fusion," Phil. Trans. R. Soc. A **378**(2184), 20200015 (2020).
19. N. Miyanaga, H. Azechi, K. A. Tanaka, T. Kanabe, T. Jitsuno, J. Kawanaka, Y. Fujimoto, R. Kodama, H. Shiraga, K. Knodo, K. Tsubakimoto, H. Habara, J. Lu, G. Xu, N. Morio, S. Matsuo, E. Miyaji, Y. Kawakami, Y. Izawa, and K. Mima, "10-kJ PW laser for the FIREX-I program," J. Phys. IV **133**(1), 81–87 (2006).
20. Optenso, "OpTaliX software for optical design, thin-films and illumination," http://www.http://optenso.com/.
21. L. Labate, P. Ferrara, L. Fulgentini, and L. A. Gizzi, "Effects of small misalignments on the intensity and Strehl ratio for a laser beam focused by an off-axis parabola," Appl. Opt. **55**(23), 6506–6515 (2016).
22. T. Ikeda, Y. Kaneyasu, H. Hosokawa, K. Shigemori, T. Norimastu, M. C. Raduban, K. Nagai, S. Kojima, Y. Abe, E. Miura, Y. Kitagawa, M. Takemura, W. Yubo, D. Jinyuan, G. Shuwang, S. Asano, R. Takizawa, S. Fujioka, H. Shiraga, Y. Arikawa, T. Ozaki, A. Iwamoto, H. Sakagami, H. Sawada, Y. Mori, and K. Yamanoi, "Fabrication of high-concentration Cu-doped deuterated targets for fast ignition experiments," Nucl. Fusion **49**(9), 095028 (2009).
23. A. L. Meadowcroft, C. D. Bentley, and E. N. Stott, "Evaluation of the sensitivity and fading characteristics of an image plate system for x-ray diagnostics," Rev. Sci. Instrum. **79**(11), 113102 (2008).
24. T. Ozakli, Y. Abe, Y. Arikawa, S. Okihara, E. Miura, A. Sunahara, K. Ishii, R. Hanayama, O. Komeda, Y. Sentoku, A. Iwamoto, H. Sakagami, T. Johzaki, J. Kawanaka, S. Tokita, N. Miyanaga, T. Jitsuno, Y. Nakata, K. Tsubakimoto, Y. Mori, and Y. Kitagawa, "Hot electron and ion spectra in axial and transverse laser irradiation in the GXII-LFEX direct fast ignition experiment," Plasma Fusion Res. **16**(0), 2404076 (2021).
25. Y. Abe, H. Hosoda, Y. Arikawa, T. Nagai, S. Kojima, S. Sakata, H. Inoue, Y. Iwasa, and K. Iwano, GEKKO-XII & LFEX Team, S. Fujioka, H. Shiraga, M. Nakai, T. Norimatsu, and H. Azechi, "Development of multichannel time-of-flight neutron spectrometer for the fast ignition experiment," Plasma Fusion Res. **9**(0), 4404110 (2014).
26. S. C. Wilks and W. L. Kruer, "Absorption of ultrashort, ultra-intense laser light by solids and overdense plasmas," IEEE J. Quantum Electron. **33**(11), 1954–1968 (1997).
27. Y. Abe, T. Johzaki, A. Sunahara, Y. Arikawa, T. Ozaki, K. Ishii, R. Hanayama, S. Okihara, E. Miura, O. Komeda, S. Sakata, K. Matsuo, H. Morita, R. Takizawa, R. Mizutani, A. Iwamoto, H. Sakagami, Y. Sentoku, H. Shiraga, M. Nakai, S. Fujioka, Y. Mori, and Y. Kitagawa, "Monte Carlo particle collision model for qualitative analysis of neutron energy spectra from anisotropic inertial confinement fusion," High Energy Density Phys. **36**, 100803 (2020).